

Structural and magnetic properties of dinuclear Cu(II) complexes featuring triazolyl-naphthalimide ligands

Jonathan A. Kitchen, Ningjin Zhang, Anthony B. Carter, Anthony J. Fitzpatrick & Grace G. Morgan

To cite this article: Jonathan A. Kitchen, Ningjin Zhang, Anthony B. Carter, Anthony J. Fitzpatrick & Grace G. Morgan (2016): Structural and magnetic properties of dinuclear Cu(II) complexes featuring triazolyl-naphthalimide ligands, Journal of Coordination Chemistry, DOI: [10.1080/00958972.2016.1193168](https://doi.org/10.1080/00958972.2016.1193168)

To link to this article: <http://dx.doi.org/10.1080/00958972.2016.1193168>



View supplementary material [↗](#)



Accepted author version posted online: 26 May 2016.
Published online: 09 Jun 2016.



Submit your article to this journal [↗](#)



Article views: 13



View related articles [↗](#)



View Crossmark data [↗](#)

Structural and magnetic properties of dinuclear Cu(II) complexes featuring triazolyl-naphthalimide ligands

Jonathan A. Kitchen^a, Ningjin Zhang^a, Anthony B. Carter^a, Anthony J. Fitzpatrick^b and Grace G. Morgan^b

^aChemistry, Faculty of Natural and Environmental Sciences, Highfield Campus, University of Southampton, Southampton, UK; ^bSchool of Chemistry, University College Dublin, Dublin, Ireland

ABSTRACT

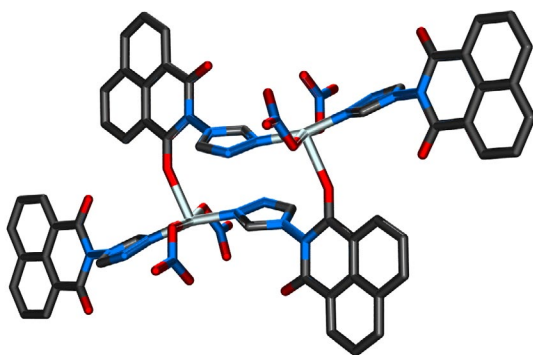
Naphthalimide-based ligands have received significant attention for their ability to act as secondary building units for metal containing network structures. The potentially bridging 1,2,4-triazole containing *N*-(1,2,4-triazolyl)-1,8-naphthalimide (**L**₁) and *N*-(1,2,4-triazolyl)-4-dimethylamino-1,8-naphthalimide (**L**₂) were prepared, characterized, and complexed with Cu(II) salts. **L**₁ resulted in crystallographically characterized dinuclear complexes, [Cu₂(**L**₁)₄(NO₃)₄] and [Cu₂(**L**₁)₂(OAc)₄] when reacted with Cu(NO₃)₂ and Cu₂(OAc)₄, respectively. Packing interactions are dominated by $\pi \cdots \pi$ and anion $\cdots \pi$ interactions and gave rise to structure extension through weak supramolecular interactions. Solid state EPR and magnetism measurements on [Cu₂(**L**₁)₄(NO₃)₄] revealed the expected values for a non-magnetically coupled square-based pyramidal dimer structure, while [Cu₂(**L**₁)₂(OAc)₄] showed strong anti-ferromagnetic coupling ($J_{\text{Cu-Cu}} = -185.6 \text{ cm}^{-1}$).

ARTICLE HISTORY

Received 24 February 2016
Accepted 5 April 2016

KEYWORDS


Naphthalimide; Cu(II);
magnetism; triazole;
supramolecular



1. Introduction

N-Substituted-1,8-naphthalimide derivatives have been utilized in a range of applications from fluorescent dyes through their more recent use in magnetically interesting, metal containing extended network structures [1–4]. In this, their π -deficient character has been exploited giving systems where

CONTACT Jonathan A. Kitchen ✉ J.A.Kitchen@soton.ac.uk

 Supplemental data for this article can be accessed at <http://dx.doi.org/10.1080/00958972.2016.1193168>.

© 2016 Informa UK Limited, trading as Taylor & Francis Group

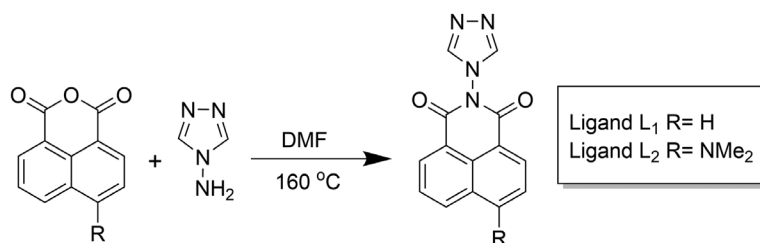
the extension of structure arises through π -based ($\pi\cdots\pi$ stacking, anion $\cdots\pi$ interactions and $C=O\cdots\pi$ interactions) contacts and results in frameworks constructed from less traditional weak non-covalent supramolecular interactions rather than the more typical charge-assisted coordination bonds observed in coordination polymers and metal-organic frameworks. Reger and co-workers have been instrumental in this field and have developed many 1,8-naphthalimide transition metal conjugates with a range of coordinating groups [4–21] whose structures were extended in the solid state by means of the naphthalimide groups acting as secondary building units through π -based interactions. Such self-assembled systems have applications in areas including molecular electronics, porous materials for sensing and gas storage, supramolecular spintronics, and crystal engineering development [22, 23]. Given our interests in the development of magnetically interesting transition metal systems [24–31] and our interests in the development of naphthalimide containing systems [32–34], we have combined 1,2,4-triazole coordination chemistry with 1,8-naphthalimide chemistry to generate two new ligands (**L**₁ and **L**₂, scheme 1) that show excellent structure extension through π -based interactions as well as interesting coordination chemistry. These naphthalimide-triazolyl systems are also ideal for the generation of multi-functional architectures as the ligand strands also show excellent fluorescent properties (*i.e.* **L**₂ is highly emissive) therefore, emissive framework materials, ideal for sensors, can potentially be generated.

Herein, we describe the synthesis, characterization, coordination chemistry and structural analysis of two novel naphthalimide-based ligands **L**₁ and **L**₂. In line with our previous studies [35], our primary aim was to probe the ability of **L**₁ and **L**₂ to develop higher order supramolecular architectures in combination with metal salts and here we have employed Cu(II) for this purpose. In doing so, we have shown that these simple ligands generate systems where structure extension occurs through $\pi\cdots\pi$ and anion $\cdots\pi$ interactions.

2. Experimental

2.1. Materials and instrumentation

All chemicals were purchased from commercial sources and used as received. Solvents were HPLC grade and were used without purification. 4-(Dimethylamino)-1,8-naphthalic anhydride was prepared from the reaction of 4-bromo-1,8-naphthalic anhydride with dimethylamine using published procedures [33]. Infrared spectra were recorded on a Thermo Scientific Nicolet iS10 spectrometer with Smart ITR accessory between 400 and 4000 cm^{-1} . NMR spectra were recorded on a Bruker DPX400 NMR spectrometer at 300 K. Chemical shifts are reported in parts per million and referenced to the residual solvent peak ($(\text{CD}_3)_2\text{SO}$: ^1H δ 2.50 ppm, ^{13}C δ 39.52 ppm). Standard conventions indicating multiplicity were used: m = multiplet, t = triplet, d = doublet, s = singlet. Mass spectrometry samples were analyzed using a MaXis (Bruker Daltonics, Bremen, Germany) mass spectrometer equipped with a time of flight analyzer. Samples were introduced to the mass spectrometer via a Dionex Ultimate 3000 autosampler and uHPLC pump [gradient 20% acetonitrile (0.2% formic acid) to 100% acetonitrile (0.2% formic acid) in five minutes at 0.6 mL min. Column: Acquity UPLC BEH C18 (Waters) 1.7 micron 50×2.1 mm]. High-resolution mass spectra were recorded using positive/negative ion electrospray ionization. UV–vis absorption



Scheme 1. Synthetic protocol for **L**₁ and **L**₂.

spectra were recorded on an Agilent Technologies Cary100 Spectrometer between 200 and 800 nm. Fluorescence measurements were carried out using an Agilent Technologies Cary Eclipse fluorescence spectrophotometer. Variable temperature magnetic susceptibility for polycrystalline powder samples were recorded on a Quantum Design MPMS[®] XL-7 SQUID magnetometer at 0.1 T. Magnetic susceptibility was recorded in the range of 300–4 K cooling at 3 K min⁻¹. The diamagnetism of the sample and sample holder were accounted for using Pascal constants and by measurement, respectively. The EPR spectra were collected at 77 K using a Magnetech ms200 X-band EPR working at 9.381 GHz with magnetic field centered at 300 mT and a field sweep of 400 mT. A modulation amplitude of 0.5 mT was used in conjunction with a microwave power of 0.1 mW and a gain of 10. Single-crystal X-ray diffraction data were either collected at 100 K on a Rigaku AFC12 goniometer equipped with an enhanced sensitivity (HG) Saturn 724+ detector mounted at the window of an FR-E+ Superbright Mo-K_α rotating anode generator ($\lambda = 0.71075$ Å) with HF or VHF varimax optics, or a Rigaku 007 HF diffractometer equipped with an enhanced sensitivity Saturn 944+ detector with a Cu-K_α rotating anode generator ($\lambda = 1.5418$ Å) with HF varimax optics [36]. Unit cell parameters were refined against all data and an empirical absorption correction applied in either CrystalClear [37] or CrysalisPro [38]. All structures were solved by direct methods using SHELXS-2013 [39] and refined on F_o^2 by SHELXL-2013 [39] using Olex2 [40]. All hydrogens were positioned geometrically and refined using a riding model with $d(\text{CH}) = 0.95$ Å, $U_{\text{iso}} = 1.2$ Ueq (C) for aromatic protons. The crystallographic data are summarized below. CCDC entries 1451355–1451358 contain the crystallographic data for the structures reported in this article.

2.2. Synthesis of L_1

1,8-Naphthalic anhydride (1.570 g, 8.0 mmol) and 4-amino-4*H*-1,2,4-triazole (0.706 g, 8.0 mmol) were added to DMF (16 mL) to give a suspension. The off-white reaction mixture was stirred at 160 °C under nitrogen for 8 h. The resulting reaction mixture was then cooled and distilled water (20 mL) was added giving a voluminous white precipitate. The resulting solid was isolated by filtration and washed by distilled water (2 × 50 mL). The solid was recrystallized from hot methanol and dried to give an off-white solid, 0.9 g (43%). Mass Spec. (HR, ESI⁺) m/z : 265.0715 ($[\text{L}_1 + \text{H}]^+$, $\text{C}_{14}\text{H}_9\text{N}_4\text{O}_2$ requires 265.0720), 287.0532 ($[\text{L}_1 + \text{Na}]^+$, $\text{C}_{14}\text{H}_8\text{N}_4\text{O}_2\text{Na}$ requires 287.0539). IR(neat): ν (cm⁻¹): 3134.3, 3059.7, 1719.9 (C=O), 1674.4 (C=O), 1580.1, 1574.8, 1440.2 (C=N), 1390.1 (C=N), 1061.6 (C–N), 1116.3 (C–N), 1175.8 (C–N), 1026.6. UV–vis λ_{max} MeCN 340 nm; λ_{max} CHCl_3 334 nm ¹H NMR (DMSO-*d*₆, 400 MHz) δ ppm: 7.98 (dd, 2H, Naphth–H), 8.62 (d, 4H, 2xNaphth–H), 8.82 (s, 2H, Triazole–H). ¹³C{¹H} NMR (DMSO-*d*₆, 101 MHz) δ ppm: 122.0, 127.9, 128.0, 132.0, 132.3, 136.3, 143.7, 161.7.

X-ray quality colorless plate-like single crystals (0.12 × 0.07 × 0.04 mm) of L_1 were grown by slow evaporation of DMF. Crystal data: $\text{C}_{14}\text{H}_8\text{N}_4\text{O}_2$ ($M = 264.25$ g mol⁻¹): monoclinic, space group $P2_1/c$ (No. 14), $a = 11.406(2)$ Å, $b = 15.520(3)$ Å, $c = 6.8292(14)$ Å, $\beta = 103.97(3)^\circ$, $V = 1173.2(4)$ Å³, $Z = 4$, $T = 100$ K, $\mu(\text{Mo-K}\alpha) = 0.105$ mm⁻¹, $D_{\text{calc}} = 1.4960$ g cm⁻³, 8158 reflections measured ($5.24^\circ \leq 2\theta \leq 50^\circ$), 2056 unique ($R_{\text{int}} = 0.1530$, $R_{\sigma} = 0.2543$) which were used in all calculations. The final R_1 was 0.0584 ($I > 2\sigma(I)$) and wR_2 was 0.1331 (all data).

2.3. Synthesis of L_2

4-Dimethylamino-1,8-naphthalic anhydride (1.442 g, 6.0 mmol) and 4-amino-4*H*-1,2,4-triazole (0.520 g, 6.0 mmol) were added to DMF (16 mL) to give a suspension. The orange–brown reaction mixture was stirred at 160 °C under nitrogen for 8 h. The resulting reaction mixture was then cooled and distilled water (20 mL) was added. The solid was isolated by filtration and purified by column chromatography using silica and an acetone–hexane (1 : 4) solvent mixture to elute the anhydride starting material and then pure acetone to elute L_2 . Removal of solvent *in vacuo* gave pure L_2 as an orange solid, 0.500 g (30%). Mass Spec. (HR, ESI⁺) m/z : 308.1148 ($[\text{L}_2 + \text{H}]^+$, $\text{C}_{16}\text{H}_{14}\text{N}_5\text{O}_2$ requires 308.1142). IR: ν (cm⁻¹): 3122.9, 2979.2, 2803.2, 1702.9 (C=O), 1657.3 (C=O), 1582.8, 1498.7, 1451.2, 1390.9, 1340.6 (C=N), 1316.7 (C=N), 1242.0 (C–N), 1213.7, 1176.7, 1138.3, 1129.3, 1070.3, 1063.4, 1019.5. UV–vis λ_{max} MeCN 447 nm; λ_{max}

CHCl_3 , 443 nm ^1H NMR ($\text{DMSO}-d_6$, 400 MHz) δ ppm: 3.19 (s, 6H, $\text{N}(\text{CH}_3)_2$), 7.27 (br d, 1H, Naphth-H), 7.82 (br dd, 1H, Naphth-H), 8.41 (br d, 1H, Naphth-H), 8.55 (br d, 1H, Naphth-H), 8.65 (br d, 1H, Naphth-H), 8.80 (s, 2H, triazole-H). $^{13}\text{C}\{^1\text{H}\}$ NMR ($\text{DMSO}-d_6$, 101 MHz) δ ppm: 44.9, 111.8, 113.2, 122.1, 124.4, 125.4, 130.6, 132.2, 133.7, 133.9, 158.1, 161.0, 161.9.

Orange plate-like crystals ($0.4 \times 0.3 \times 0.1$ mm) of L_2 were grown by vapor diffusion of diethyl ether into a DMF solution of L_2 . The crystal contained non-merohedral twinning [twinned data refinement scales: 0.6741(12), 0.3259(12) where component 2 rotated by 179.9712° around $[1.00 \ -0.00 \ -0.00]$ (reciprocal) or $[0.98 \ -0.00 \ 0.18]$ (direct)]. Crystal data: $\text{C}_{16}\text{H}_{13}\text{N}_5\text{O}_2$ ($M = 307.31$ g mol $^{-1}$): monoclinic, space group $P2_1/c$ (No. 14), $a = 12.0954(4)$ Å, $b = 15.9987(4)$ Å, $c = 7.0636(2)$ Å, $\beta = 96.094(3)^\circ$, $V = 1359.16(7)$ Å 3 , $Z = 4$, $T = 100$ K, $\mu(\text{Cu}-\text{K}\alpha) = 0.859$ mm $^{-1}$, $D_{\text{calc}} = 1.502$ g cm $^{-3}$, 4481 reflections measured ($13.292^\circ \leq 2\theta \leq 133.984^\circ$), 4481 unique ($R_{\text{int}} = 0.0397$, $R_\sigma = 0.0203$) which were used in all calculations. The final R_1 was 0.0380 ($I > 2\sigma(I)$) and wR_2 was 0.1099 (all data).

2.4. Synthesis of $[\text{Cu}_2(\text{L}_1)_4(\text{NO}_3)_4]$

Copper(II) nitrate trihydrate (0.024 g, 0.1 mmol) and L_1 (0.053 g, 0.2 mmol) were dissolved in CH_3CN –MeOH (1:1 – 10 mL) and heated at 60°C with continuous stirring for 6 h. The resulting blue solution was divided into four equal portions and subjected to vapor diffusion of diethyl ether at room temperature. After three days, blue crystals were obtained (0.021 g, 27%). IR: ν (cm $^{-1}$): 1704, 1590, 1536, 1470, 1397, 1308, 1291, 1230, 1173, 1140, 1118, 1077, 1016, 891, 846, 771, 726, 627, 533. Crystal data for $[\text{Cu}_2(\text{L}_1)_4(\text{NO}_3)_4]$: $\text{C}_{56}\text{H}_{32}\text{Cu}_2\text{N}_{20}\text{O}_{20}$ ($M = 1432.09$ g mol $^{-1}$): triclinic, space group $P\bar{1}$ (No. 2), $a = 8.3676(12)$ Å, $b = 13.0331(18)$ Å, $c = 13.773(2)$ Å, $\alpha = 72.508(8)^\circ$, $\beta = 80.202(11)^\circ$, $\gamma = 79.362(10)^\circ$, $V = 1397.4(4)$ Å 3 , $Z = 1$, $T = 100(2)$ K, $\mu(\text{Mo}-\text{K}\alpha) = 0.863$ mm $^{-1}$, $D_{\text{calc}} = 1.702$ g cm $^{-3}$, 15,625 reflections measured ($5.146^\circ \leq 2\theta \leq 49.998^\circ$), 4904 unique ($R_{\text{int}} = 0.0261$, $R_\sigma = 0.0296$) which were used in all calculations. The final R_1 was 0.0307 ($I > 2\sigma(I)$) and wR_2 was 0.0796 (all data).

2.5. Synthesis of $[\text{Cu}_2(\text{L}_1)_2(\text{OAc})_4]$

Copper(II) acetate monohydrate (0.041 g, 0.2 mmol) and L_1 (0.054 g, 0.2 mmol) were dissolved in CH_3CN –MeOH (1:1 – 10 mL) and heated at 60°C with continuous stirring for 8 h. The resulting blue solution was divided into four equal portions and subjected to vapor diffusion of diethyl ether resulting in the formation of blue–green crystals (0.012 g, 14%). IR: ν (cm $^{-1}$): 3472, 3369, 3266, 1707, 1600, 1435, 1420, 1354, 1326, 1233, 1222, 1172, 1138, 1114, 1051, 1032, 892, 850, 802, 776, 686, 626, 533. Crystal data: $\text{C}_{36}\text{H}_{28}\text{Cu}_2\text{N}_8\text{O}_{12}$ ($M = 891.74$ g mol $^{-1}$): monoclinic, space group $C2/c$ (No. 15), $a = 29.020(6)$ Å, $b = 8.1450(16)$ Å, $c = 18.711(4)$ Å, $\beta = 108.42(3)^\circ$, $V = 4196.1(16)$ Å 3 , $Z = 4$, $T = 100$ K, $\mu(\text{Mo}-\text{K}\alpha) = 1.081$ mm $^{-1}$, $D_{\text{calc}} = 1.412$ g cm $^{-3}$, 11,880 reflections measured ($5.506^\circ \leq 2\theta \leq 49.996^\circ$), 3673 unique ($R_{\text{int}} = 0.0252$, $R_\sigma = 0.0401$) which were used in all calculations. The final R_1 was 0.0379 ($I > 2\sigma(I)$) and wR_2 was 0.0991 (all data).

3. Results and discussion

3.1. Ligand synthesis

The ligands, 1,8-naphthalimide-1,2,4-triazole (L_1) and 4-(dimethylamino)-1,8-naphthalimide-1,2,4-triazole (L_2) were synthesized as shown in scheme 1. The reaction of one equivalent of 1,8-naphthalic anhydride or 4-dimethylamino-1,8-naphthalic anhydride with one equivalent of 4-amino-4H-1,2,4-triazole in DMF at 160°C under N_2 gave L_1 as a pure off-white solid (43%) and L_2 as a crude brown solid on addition of distilled water to the reaction mixtures. L_2 required chromatographic purification to give the pure product as an orange powder (30%). Both ligands were fully characterized using NMR spectroscopy, IR spectroscopy, UV–vis spectroscopy, and mass spectrometry (see supporting information).

^1H NMR spectra showed the expected aromatic naphthalimide protons for L_1 and L_2 (these were significantly shifted from the corresponding peaks of the starting naphthalic anhydrides) and the characteristic triazole protons at 8.8 ppm. Mass spectrometry confirmed the successful formation of L_1 and L_2 with peaks at 265.0715, m/z , and 308.1148, m/z corresponding to the $[\text{M} + \text{H}]^+$ ions for L_1 and L_2 , respectively. Additionally, a peak was observed for the $[\text{M} + \text{Na}]^+$ species of L_1 (287.0532 m/z) species.

Colorless crystals of L_1 were grown from slow evaporation of a DMF solution and the low temperature (100 K) X-ray structure was determined. L_1 crystallized in the monoclinic space group $P2_1/c$ and contained one molecule in the asymmetric unit (figure 1(A)). The triazole ring is orthogonal to the naphthalimide ring, a feature commonly observed in such ligand species, with an angle of 79° between the mean planes of the two rings. Packing interactions are dominated by $\pi \cdots \pi$ stacking interactions between neighboring naphthalimide rings (figure 1(B)) as well as weaker non-classical CH hydrogen bonding from the triazole CH groups (figure 2(A)). Neighboring molecules of L_1 are arranged into alternating

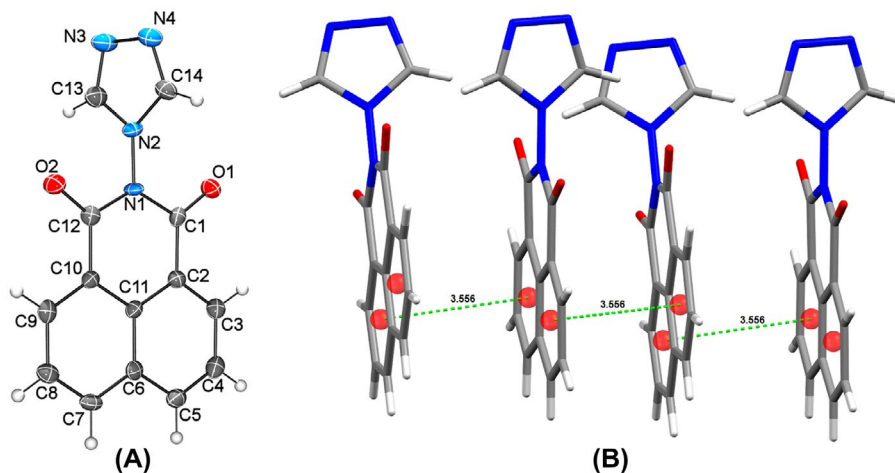


Figure 1. Molecular structure of L_1 with thermal ellipsoids at 50% probability (A). Packing of L_1 showing $\pi \cdots \pi$ stacking between molecules (B).

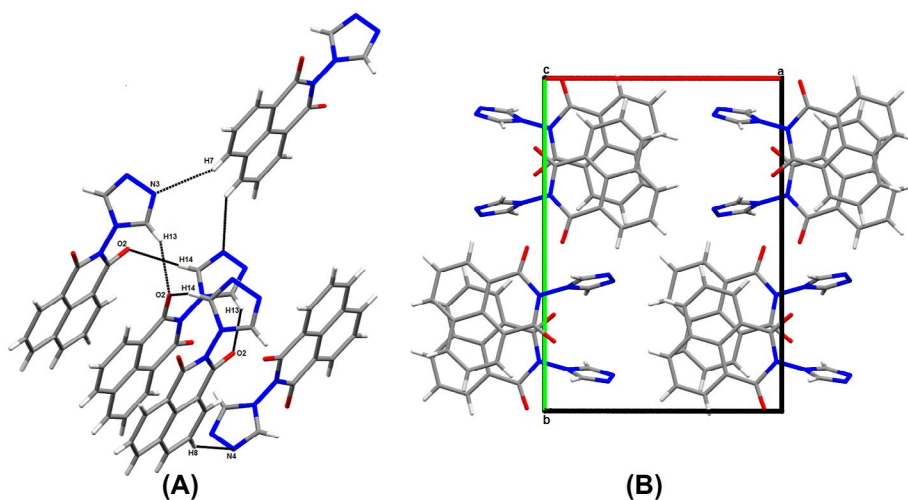


Figure 2. View of C–H based hydrogen-bonding interactions in L_1 (A). Packing of L_1 showing π -stacked chains in the crystallographic b direction (B).

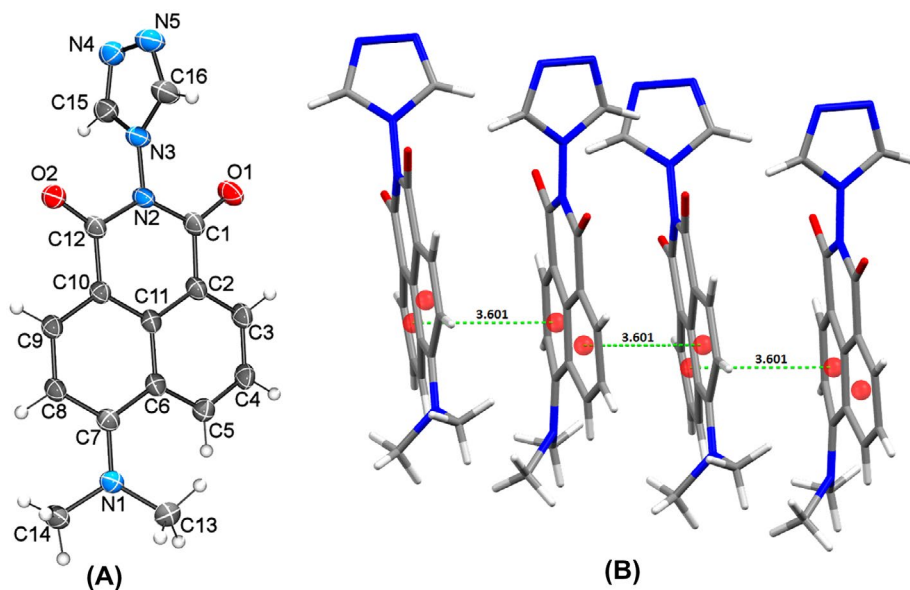


Figure 3. Molecular structure of L_2 with thermal ellipsoids at 50% probability (A). Packing of L_2 showing $\pi \cdots \pi$ stacking between molecules (B).

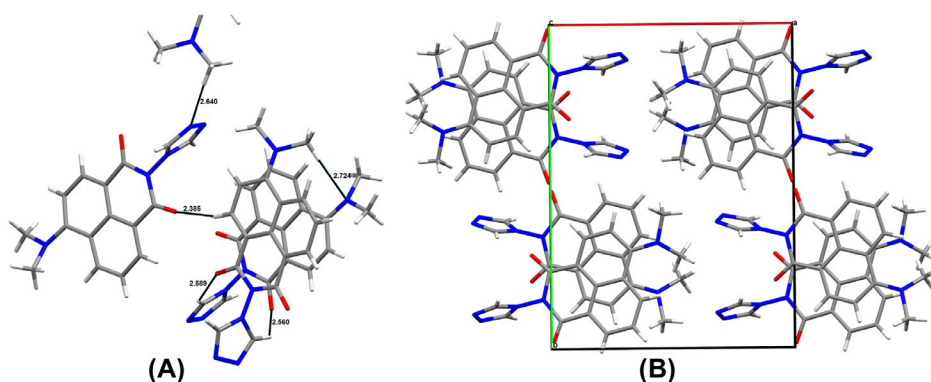


Figure 4. View of C–H based hydrogen-bonding interactions in L_2 (A). Packing of L_2 showing π stacked chains in the crystallographic b direction (B).

stacks through strong $\pi \cdots \pi$ stacking interactions [centroid \cdots centroid = 3.632 Å and centroid \cdots central naphtha-C = 3.414 Å]. These alternating stacks are then linked to neighboring stacks through weaker $CH \cdots O$ and $CH \cdots N$ hydrogen bonding.

Small orange crystals of L_2 were grown from slow evaporation of a DMF solution and the low temperature (100 K) X-ray structure was determined. The crystal contained non-merohedral twinning where one component was rotated by *ca.* 180°. L_2 crystallized in the monoclinic space group $P2_1/c$ with one molecule in the asymmetric unit (figure 3(A)). The triazole ring in L_2 is perpendicular to the naphthalimide ring plane (81°), and the packing interactions are again dominated by $\pi \cdots \pi$ stacking interactions between neighboring naphthalimide rings [centroid \cdots centroid = 3.601 Å, figure 3(B)] as well as weaker non-classical CH hydrogen bonding from the triazole CH groups (figure 4(A)).

The solid state packing interactions present in both L_1 and L_2 involve $\pi \cdots \pi$ stacking between neighboring naphthalimide units, and with these being the dominant interaction, we expect this

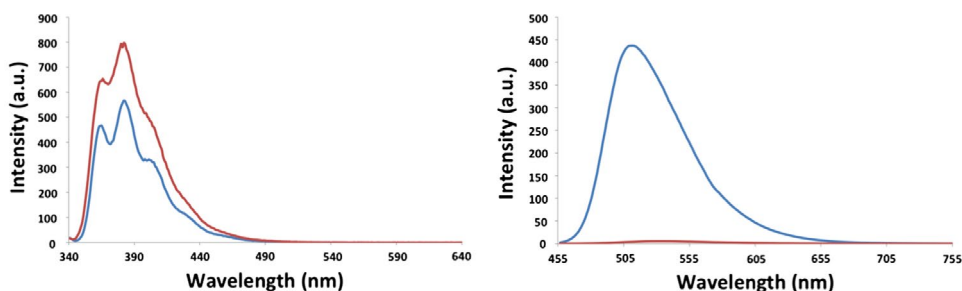


Figure 5. Emission spectra of **L**₁ (left) and **L**₂ (right) in CHCl₃ (blue) and MeCN (red) (see <http://dx.doi.org/10.1080/00958972.2016.1193168> for color version).

same interaction to be present in subsequent coordination complexes. Therefore, these ligand species should be ideal for the preparation of new metal-based supramolecular architectures where the structure directing properties of the ligands might influence the physical properties (e.g. magnetism or photophysical properties) of the metal centers.

The absorption and the emission properties of **L**₁ and **L**₂ were briefly investigated and were typical for 1,8-naphthalimide-based compounds [1]. Both **L**₁ and **L**₂ displayed high-energy absorptions in the 200–250 nm range, typical for such organic species. **L**₁ displayed a broad absorption band with λ_{max} at 340 nm, while for **L**₂ this broad absorption had λ_{max} at 440 nm (attributed to an ICT band) when recorded in CHCl₃ and MeCN. Upon excitation at λ_{max} , both **L**₁ and **L**₂ show broad fluorescence emission (figure 5). **L**₁ displayed emission with λ_{max} at 380 nm when excited at 340 nm in both CHCl₃ and MeCN, whereas **L**₂ displayed broad emission at 511 and 532 nm when excited at 440 nm in CHCl₃ and MeCN, respectively.

3.2. Coordination chemistry of **L**₁ and **L**₂

L₁ and **L**₂ were reacted with Cu(II) salts [Cu(NO₃)₂, Cu(OAc)₂, CuSO₄] in a range of solvents and with a range of M:L ratios in order to assess their coordination ability and determine the effect that the naphthalimide group has on the packing in the solid state structures. Despite many attempts, the only sets of reaction conditions that gave bulk samples of single crystals were Cu(NO₃)₂·3H₂O with **L**₁ in a 1:2 ratio in MeCN/MeOH (1:1) and Cu(OAc)₂ with **L**₁ in a 1:1 ratio in MeCN/MeOH (1:1). The reaction of two equivalents of **L**₁ and one equivalent of Cu(NO₃)₂ at 60 °C in MeCN/MeOH (1:1) for 1 h gave a clear blue solution that upon cooling to room temperature was subjected to vapor diffusion of diethyl ether. After 3 days, a number of blue crystals of [Cu₂(**L**₁)₄(NO₃)₄] were obtained (27%). Reaction of Cu(OAc)₂ with **L**₁ gave a very small number of blue single crystals suitable for diffraction studies. The resulting molecular structure was found to be a paddle wheel Cu(II) dimer of [Cu₂(**L**₁)₂(OAc)₄]. To date, reactions involving either CuSO₄ or **L**₂ have not resulted in any crystalline samples.

3.3. Crystallographic analysis of [Cu₂(**L**₁)₄(NO₃)₄]

[Cu₂(**L**₁)₄(NO₃)₄] crystallized in the triclinic space group $P\bar{1}$ and contained half of a molecule in the asymmetric unit with the other half generated by a center of inversion (figure 6, table 1).

The result is a dimeric complex where each copper(II) is coordinated with two nitrogen atoms from different triazole groups, two nitrate oxygen atoms, and one naphthalimide carbonyl oxygen atom from a symmetry generated naphthalimide to give an overall N₂O₄ coordination sphere (figure 6). Analysis of the coordination geometry around Cu(II) reveals the degree of trigonality (τ) to be 0.06, which is consistent with a slightly distorted square–pyramidal coordination environment. Bond lengths and angles are consistent with other axially elongated square-based pyramidal structures where the equatorial (square base) bond lengths average 1.985(2) Å, whilst the axial bond to the carbonyl oxygen atom is

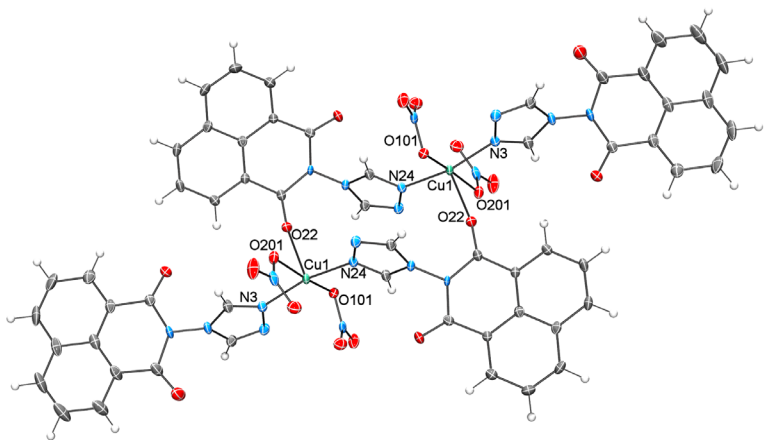


Figure 6. Molecular structure of [Cu₂(L₁)₄(NO₃)₄] with thermal ellipsoids set at 50%.

Table 1. Selected bond lengths (Å) and angles (°) for [Cu₂(L₁)₄(NO₃)₄].

Cu(1)–O(201)	1.9724(15)
Cu(1)–O(101)	1.9866(15)
Cu(1)–N(3)	1.9891(16)
Cu(1)–N(24) ^a	1.9906(16)
Cu(1)–O(22)	2.3068(15)
Cu(1)–Cu(1) ^a	6.4799 (11)
O(201)–Cu(1)–O(101)	169.93(6)
O(201)–Cu(1)–N(3)	87.88(7)
O(101)–Cu(1)–N(3)	90.41(6)
O(201)–Cu(1)–N(24) ^a	93.28(6)
O(101)–Cu(1)–N(24) ^a	90.70(6)
N(3)–Cu(1)–N(24) ^a	166.46(7)
O(201)–Cu(1)–O(22)	82.07(6)
O(101)–Cu(1)–O(22)	88.03(6)
N(3)–Cu(1)–O(22)	90.59(6)
N(24) ^a –Cu(1)–O(22)	102.94(6)

^a–x + 1, –y + 2, –z.

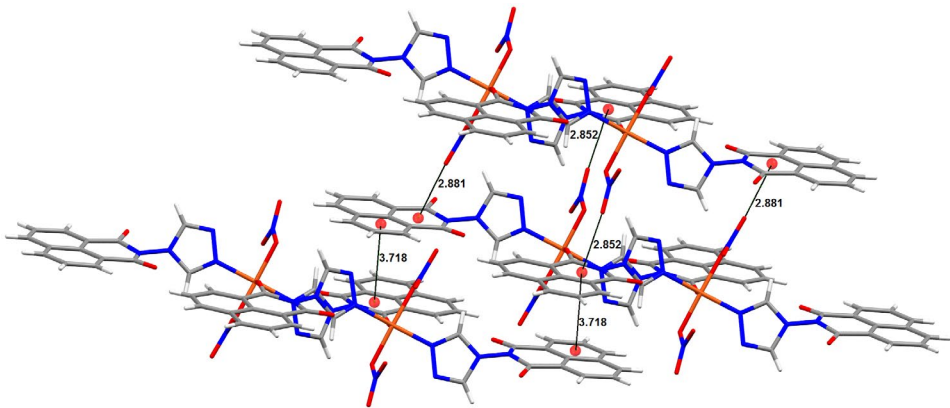


Figure 7. Packing interactions of [Cu₂(L₁)₄(NO₃)₄] showing π···π stacking and non-classical interaction between molecules.

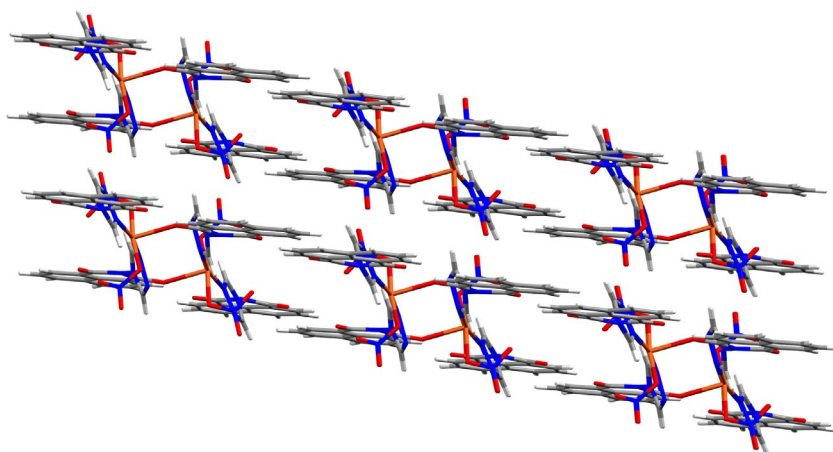


Figure 8. Long range order of $[\text{Cu}_2(\text{L}_1)_4(\text{NO}_3)_4]$ showing the chains of dimers along the crystallographic a axis.

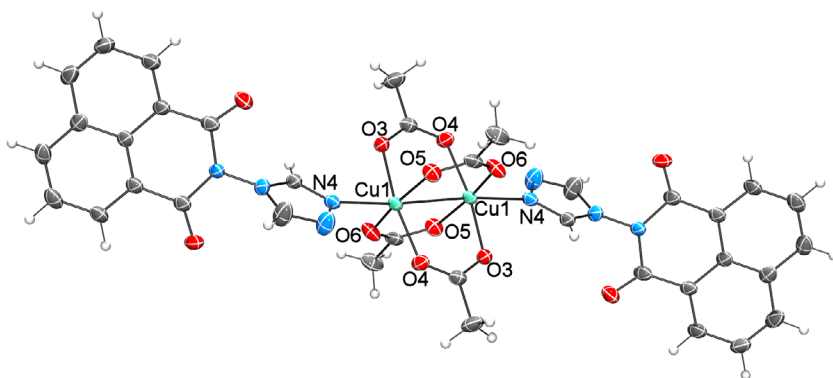


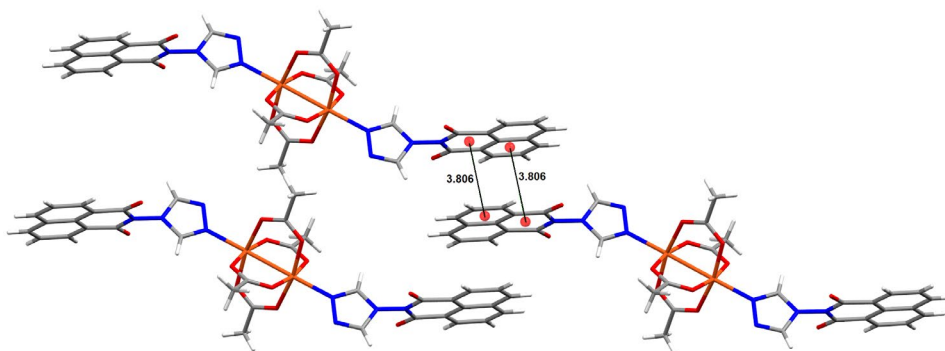
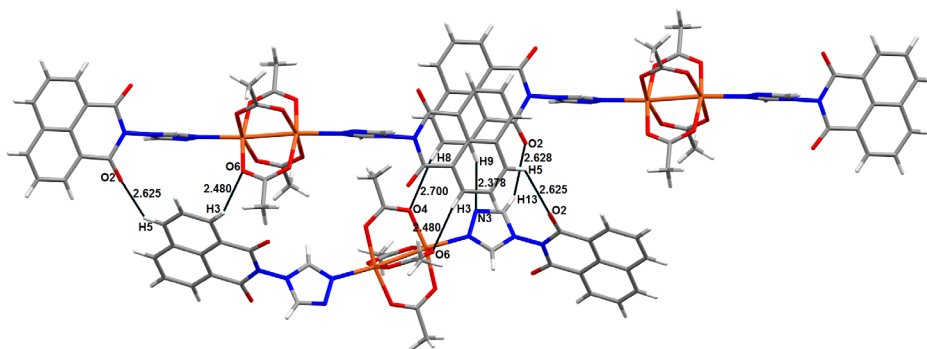
Figure 9. Molecular structure of $[\text{Cu}_2(\text{L}_1)_2(\text{OAc})_4]$ with thermal ellipsoids set at 50%.

2.307(2) Å. The coordination of the carbonyl oxygen atoms in naphthalimides to transition metals is not a commonly observed occurrence and only three structures are reported in the CSD [19, 41, 42]. The naphthalimide ligand that bridges the two copper(II) centers gives rise to a 14-membered ring involving the two copper(II) centers and shows strong $\pi \cdots \pi$ stacking between the neighboring triazole rings [centroid \cdots centroid = 3.517 Å].

Packing interactions in $[\text{Cu}_2(\text{L}_1)_4(\text{NO}_3)_4]$ are dominated by strong anion $\cdots\pi$ and face-to-face $\pi \cdots \pi$ stacking interactions. Anion $\cdots\pi$ interactions exist between two neighboring dimers where the distal oxygen atoms of the coordinated nitrate anions are involved in anion $\cdots\pi$ interactions to the imide rings of neighboring dimers (figure 7) with O \cdots centroid distances of 2.881 and 2.852 Å for the two different interactions. The interactions are self-complementary so there are four interactions in total between two dimers and this extends them into chains of dimers in the direction of the crystallographic a -axis (figure 8). These anion $\cdots\pi$ linked chains are linked to neighboring chains via offset face-to-face $\pi \cdots \pi$ stacking between naphthalene rings where all four naphthalimide ligands are involved in stacking interactions to link the chains [centroid \cdots centroid distances = 3.718].

Table 2. Selected bond lengths (Å) and angles (°) for $[\text{Cu}_2(\text{L}_1)_2(\text{OAc})_4]$.

Cu(1)–O(3)	1.9758(18)
Cu(1)–O(4)	1.9648(18)
Cu(1)–O(5)	1.9657(19)
Cu(1)–O(6)	1.9638(19)
Cu(1)–N(4)	2.181(2)
Cu(1)–Cu(1) ^a	2.6511(11)
O(3)–Cu(1)–N(4)	90.95(8)
O(4) ^b –Cu(1)–O(3)	168.32(8)
O(4) ^b –Cu(1)–O(5)	90.35(8)
O(4) ^b –Cu(1)–N(4)	100.72(8)
O(5)–Cu(1)–O(3)	89.21(8)
O(5)–Cu(1)–N(4)	93.98(8)
O(6)–Cu(1)–O(3)	88.76(8)
O(6)–Cu(1)–O(4) ^a	89.31(8)
O(6)–Cu(1)–O(5)	168.30(8)
O(6)–Cu(1)–N(4)	97.58(8)

^a1 – x, –y, 1 – z.**Figure 10.** Packing of $[\text{Cu}_2(\text{L}_1)_2(\text{OAc})_4]$ showing $\pi \cdots \pi$ stacking between molecules.**Figure 11.** Packing of $[\text{Cu}_2(\text{L}_1)_2(\text{OAc})_4]$ showing non-classical interaction between molecules.

3.4. Crystallographic analysis of $[\text{Cu}_2(\text{L}_1)_2(\text{OAc})_4]$

$[\text{Cu}_2(\text{L}_1)_2(\text{OAc})_4]$ crystallized in the monoclinic space group $C2/c$ and contained half of one molecule in the asymmetric unit with the other half generated by a center of inversion (figure 9, table 2).

The resulting paddle wheel dimer consists of two Cu(II) centers bridged by four acetate molecules and capped with two L_1 molecules to give O_4N coordination environments around each copper atom.

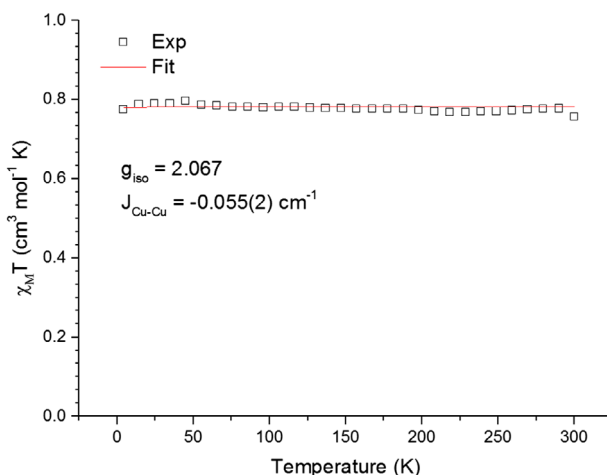


Figure 12. Plot of $\chi_M T$ versus T for $[\text{Cu}_2(\text{L}_1)_4(\text{NO}_3)_4]$ between 4 and 300 K.

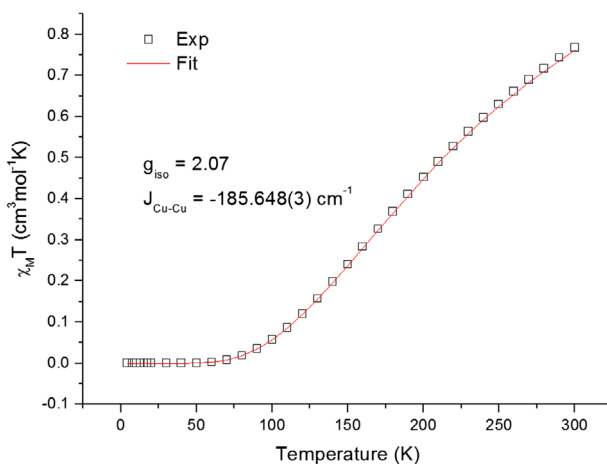


Figure 13. Plot of $\chi_M T$ versus T for $[\text{Cu}_2(\text{L}_1)_2(\text{OAc})_4]$ between 4 and 300 K.

The Cu(II) ions are 2.651(2) Å apart, similar to other copper paddle wheel complexes [35]. The copper ions adopt a near perfect square-based pyramidal geometry with the degree of trigonality (τ) being 0 [43]. Bond lengths and angles are also consistent with other axially elongated square-based pyramidal structures where the equatorial acetate oxygen Cu–O bond lengths average 1.968(2) Å, whilst the axial triazole nitrogen atom Cu–N bond length is 2.180(2) Å (table 2).

Packing interactions in $[\text{Cu}_2(\text{L}_1)_2(\text{OAc})_4]$ also involve the naphthalimide π -system, as well as CH hydrogen bonding involving the somewhat acidic triazole CH moiety (a commonly observed packing interaction in such structures) [44]. Paddle wheel dimer units are packed into *pseudo* 1-D chains through face-to-face $\pi \cdots \pi$ stacking between neighboring naphthalimide moieties [centroid \cdots centroid = 3.806 Å] (figure 10). These chains are then linked to neighboring chains through weak CH hydrogen bonding between triazole CH and naphthalimide C=O groups [C \cdots O = 3.458 Å and $\angle(\text{CH} \cdots \text{O}) = 147^\circ$] (figure 11).

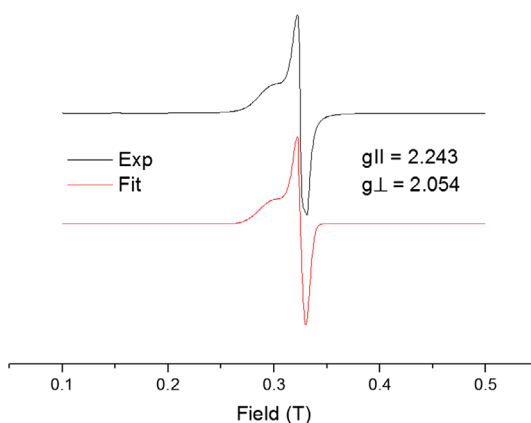


Figure 14. Solid state X-band EPR spectrum of $[\text{Cu}_2(\text{L}_1)_4(\text{NO}_3)_4]$ measured at 77 K (black) and the calculated fit (red) (see <http://dx.doi.org/10.1080/00958972.2016.1193168> for color version).

3.5. Magnetism and EPR studies

Variable temperature magnetic susceptibility measurements were obtained for polycrystalline powder samples of $[\text{Cu}_2(\text{L}_1)_4(\text{NO}_3)_4]$ and $[\text{Cu}_2(\text{L}_1)_2(\text{OAc})_4]$ and are shown in figures 12 and 13, respectively. The $\chi_M T$ value of just below $0.8 \text{ cm}^3 \text{ mol}^{-1} \text{ K}$ for $[\text{Cu}_2(\text{L}_1)_4(\text{NO}_3)_4]$ across the entire temperature range is representative of a Cu(II) dimer with negligible magnetic interaction between the Cu(II) centers. In the plot for $[\text{Cu}_2(\text{L}_1)_2(\text{OAc})_4]$, the $\chi_M T$ value decreases on cooling from 0.8 to $0 \text{ cm}^3 \text{ mol}^{-1} \text{ K}$ indicative of antiferromagnetic coupling.

The solid state X-band EPR spectrum of $[\text{Cu}_2(\text{L}_1)_4(\text{NO}_3)_4]$, measured at 77 K, also showed negligible interaction between the Cu(II) ions (figure 14). The g factor derived from the data are 2.07 and is in line with square-pyramidal geometry. There are no obvious hyperfine interactions from the triazole ^{14}N nuclei. There was no EPR signal at 77 K at X-band for $[\text{Cu}_2(\text{L}_1)_2(\text{OAc})_4]$, presumably due to the large anti-ferromagnetic coupling between the Cu(II) ions coupled with the sensitivity of the X-band EPR used.

Both the magnetic and EPR data for $[\text{Cu}_2(\text{L}_1)_4(\text{NO}_3)_4]$ and the magnetic data for $[\text{Cu}_2(\text{L}_1)_2(\text{OAc})_4]$ were fitted using the program PHI [45] utilizing the Hamiltonian:

$$\hat{H} = -2 \sum_{i < j}^{i,j \in N} \vec{S}_i \cdot \vec{J}_{ij} \cdot \vec{S}_j - g\mu_B \sum_i \vec{B} \cdot \vec{S}_i$$

The resulting fit gave a g_{iso} of 2.067 and a $J_{\text{Cu-Cu}} = -0.05 \text{ cm}^{-1}$ this correlates well with the very weakly interacting Cu(II) ion model. This is not unexpected as the Cu(II) centers were shown to be $\sim 6.5 \text{ \AA}$ apart (see above).

Conversely, for $[\text{Cu}_2(\text{L}_1)_2(\text{OAc})_4]$, the fit gave g_{iso} of 2.07 and $J_{\text{Cu-Cu}} = -185.6 \text{ cm}^{-1}$ consistent with a strongly anti-ferromagnetic interaction between the Cu(II) centers. $[\text{Cu}_2(\text{L}_1)_2(\text{OAc})_4]$ was EPR silent, further emphasizing the strong anti-ferromagnetic coupling between the metal centers.

4. Conclusion

The syntheses of two new 1,8-naphthalimide-1,2,4-triazolyl-based ligands, L_1 and L_2 , were achieved and the solid state packing revealed significant π -based interactions. Coordination chemistry was attempted using Cu(II) salts in the hope that the π -based interactions would be the dominant intermolecular interaction and allow for functional metal-organic networks to be constructed using supramolecular self-assembly. $\text{Cu}(\text{NO}_3)_2$ when reacted with L_1 gave single crystals of a dimeric complex $[\text{Cu}_2(\text{L}_1)_4(\text{NO}_3)_4]$, whilst reaction of L_1 with $\text{Cu}_2(\text{OAc})_4$ gave the paddle wheel dimer $[\text{Cu}_2(\text{L}_1)_2(\text{OAc})_4]$. The expected π -based

interactions were also present in the complex and resulted in extension of the structure into a supra-molecular metal-organic network. EPR and magnetism measurements of $[\text{Cu}_2(\text{L}_1)_4(\text{NO}_3)_4]$ showed very little coupling between the square-based pyramidal Cu(II) centers, however the interaction between the Cu(II) centers in $[\text{Cu}_2(\text{L}_1)_2(\text{OAc})_4]$ was strongly anti-ferromagnetic. The use of naphthalimide-based ligands and triazole coordination sites has resulted in metal-organic supramolecular networks where interesting dimer complexes were assembled into extended networks through non-covalent $\pi \cdots \pi$ and anion $\cdots \pi$ interactions. These initial results suggest that L_1 and L_2 (and subsequent derivatives) could be ideal for developing magnetically interesting self-assembled systems, a rapidly expanding area in molecular electronics research and multi-functional devices. Such research requires modular ligand design so that a range of functional groups to fine-tune the system or allow for immobilization of assemblies can be readily incorporated and so that predictable intermolecular interactions can be generated, all properties that these triazole-naphthalimide systems possess.

Supplementary material

Supporting information is available for this article. CCDC entries 1451355–1451358 contain the crystallographic data for the structures reported in this article. All data supporting this study are openly available from the University of Southampton repository at <http://dx.doi.org/10.5258/SOTON/390630>.

Acknowledgments

The authors are grateful to the University of Southampton and University College Dublin for support of this work. J.A.K. thanks the EPSRC for funding through grant reference EP/K039466/1. In addition G.G.M. and A.J.F. thank Science Foundation Ireland for an Investigator Project Award 12/IP/1703 (to G.G.M.), the National University of Ireland and the Cultural Service of the French Embassy in Ireland for scholarships (to A.J.F.) and the Irish Higher Education Authority for funding for a SQUID magnetometer.

Disclosure statement

No potential conflict of interest was reported by the authors.

Funding

This work was supported by the Engineering and Physical Sciences Research Council [grant number EP/K039466/1]; Science Foundation Ireland [grant number 12/IP/1703].

References

- [1] S. Banerjee, E.B. Veale, C.M. Phelan, S.A. Murphy, G.M. Tocci, L.J. Gillespie, D.O. Frimannsson, J.M. Kelly, T. Gunnlaugsson. *Chem. Soc. Rev.*, **42**, 1601 (2013).
- [2] C.J. McAdam, B.H. Robinson, J. Simpson. *Organometallics*, **19**, 3644 (2000).
- [3] R.M. Duke, E.B. Veale, F.M. Pfeffer, P.E. Kruger, T. Gunnlaugsson. *Chem. Soc. Rev.*, **39**, 3936 (2010).
- [4] D.L. Reger, A. Leitner, M.D. Smith. *Cryst. Growth Des.*, **15**, 5637 (2015).
- [5] D.L. Reger, J.D. Elgin, R.F. Semeniuc, P.J. Pellechia, M.D. Smith. *Chem. Commun.*, 4068 (2005).
- [6] D.L. Reger, A. Debreczeni, M.D. Smith, J. Jezierska, A. Ozarowski. *Inorg. Chem.*, **51**, 1068 (2012).
- [7] D.L. Reger, R.F. Semeniuc, J.D. Elgin, V. Rassolov, M.D. Smith. *Cryst. Growth Des.*, **6**, 2758 (2006).
- [8] D.L. Reger, E. Sirianni, J.J. Horger, M.D. Smith, R.F. Semeniuc. *Cryst. Growth Des.*, **10**, 386 (2010).
- [9] D.L. Reger, A. Debreczeni, B. Reinecke, V. Rassolov, M.D. Smith. *Inorg. Chem.*, **48**, 8911 (2009).
- [10] D.L. Reger, B. Reinecke, M.D. Smith, R.F. Semeniuc. *Inorg. Chim. Acta*, **362**, 4377 (2009).
- [11] D.L. Reger, J.D. Elgin, P.J. Pellechia, M.D. Smith, B.K. Simpson. *Polyhedron*, **28**, 1469 (2009).
- [12] D.L. Reger, A. Debreczeni, M.D. Smith. *Inorg. Chim. Acta*, **364**, 10 (2010).
- [13] D.L. Reger, J.J. Horger, M.D. Smith. *Chem. Commun.*, **47**, 2805 (2011).
- [14] D.L. Reger, J. Horger, M.D. Smith, G.J. Long. *Chem. Commun.*, 6219 (2009).
- [15] D.L. Reger, J.J. Horger, M.D. Smith, G.J. Long, F. Grandjean. *Inorg. Chem.*, **50**, 686 (2011).
- [16] D.L. Reger, A. Debreczeni, J.J. Horger, M.D. Smith. *Cryst. Growth Des.*, **11**, 4068 (2011).

- [17] D.L. Reger, A. Debreczeni, M.D. Smith. *Eur. J. Inorg. Chem.*, **2012**, 712 (2012).
- [18] D.L. Reger, A. Debreczeni, M.D. Smith. *Inorg. Chim. Acta*, **378**, 42 (2011).
- [19] D.L. Reger, J.J. Horger, A. Debreczeni, M.D. Smith. *Inorg. Chem.*, **50**, 10225 (2011).
- [20] D.L. Reger, A. Debreczeni, M.D. Smith. *Inorg. Chem.*, **50**, 11754 (2011).
- [21] D.L. Reger, A.P. Leitner, M.D. Smith. *Cryst. Growth Des.*, **15**, 5637 (2015).
- [22] T.R. Cook, Y.-R. Zheng, P.J. Stang. *Chem. Rev.*, **113**, 734 (2013).
- [23] G. Seeber, G.J.T. Cooper, G.N. Newton, M.H. Rosnes, D.-L. Long, B.M. Kariuki, P. Kögerler, L. Cronin. *Chem. Sci.*, **1**, 62 (2010).
- [24] A. Bhattacharjee, V. Ksenofontov, J.A. Kitchen, N.G. White, S. Brooker, P. Gütllich. *Appl. Phys. Lett.*, **92**, 174104 (2008).
- [25] G.N.L. Jameson, F. Werner, M. Bartel, A. Absmeier, M. Reissner, J.A. Kitchen, S. Brooker, A. Caneschi, C. Carbonera, J.-F. Letard, W. Linert. *Eur. J. Inorg. Chem.*, **2009**, 3948 (2009).
- [26] J.A. Kitchen, S. Brooker. *Dalton Trans.*, **39**, 3358 (2010).
- [27] J.A. Kitchen, G.N.L. Jameson, V.A. Milway, J.L. Tallon, S. Brooker. *Dalton Trans.*, **39**, 7637 (2010).
- [28] J.A. Kitchen, N.G. White, G.N.L. Jameson, J.L. Tallon, S. Brooker. *Inorg. Chem.*, **50**, 4586 (2011).
- [29] J.A. Kitchen, J. Olguín, R. Kulmaczewski, N.G. White, V.A. Milway, G.N.L. Jameson, J.L. Tallon, S. Brooker. *Inorg. Chem.*, **52**, 11185 (2013).
- [30] J.P. Byrne, J.A. Kitchen, O. Kotova, V. Leigh, A.P. Bell, J.J. Boland, M. Albrecht, T. Gunnlaugsson. *Dalton Trans.*, **43**, 196 (2014).
- [31] R. Kulmaczewski, J. Olguín, J.A. Kitchen, H.L.C. Feltham, G.N.L. Jameson, J.L. Tallon, S. Brooker. *J. Am. Chem. Soc.*, **136**, 878 (2014).
- [32] S. Banerjee, J.A. Kitchen, S.A. Bright, J.E. O'Brien, D.C. Williams, J.M. Kelly, T. Gunnlaugsson. *Chem. Commun.*, **49**, 8522 (2013).
- [33] S. Banerjee, J.A. Kitchen, T. Gunnlaugsson, J.M. Kelly. *Org. Biomol. Chem.*, **11**, 5642 (2013).
- [34] E.B. Veale, J.A. Kitchen, T. Gunnlaugsson. *Supramol. Chem.*, **25**, 101 (2013).
- [35] J.A. Kitchen, P.N. Martinho, G.G. Morgan, T. Gunnlaugsson. *Dalton Trans.*, **43**, 6468 (2014).
- [36] S.J. Coles, P.A. Gale. *Chem. Sci.*, **3**, 683 (2012).
- [37] CrystalClear-SM Expert 3.1. b27, *Rigaku* (2012).
- [38] CrysAlisPro 1.171.38.41. *Rigaku Oxford Diffraction* (2015).
- [39] G.M. Sheldrick. *Acta Crystallogr. Sect. A*, **64**, 112 (2008).
- [40] O.V. Dolomanov, L.J. Bourhis, R.J. Gildea, J.A.K. Howard, H. Puschmann. *J. Appl. Crystallogr.*, **42**, 339 (2009).
- [41] R. García-Bueno, M.D. Santana, G. Sánchez, J. García, G. García, J. Pérez, L. García. *Dalton Trans.*, **39**, 5728 (2010).
- [42] B.K. Nicholson, P.M. Crosby, K.R. Maunsell, M.J. Wyllie. *J. Organomet. Chem.*, **716**, 49 (2012).
- [43] A.W. Addison, T.N. Rao, J. Reedijk, J. van Rijn, G.C. Verschoor. *J. Chem. Soc., Dalton Trans.*, 1349 (1984).
- [44] R.M. Hellyer, J.A. Joule, D.S. Larsen, S. Brooker. *Acta Crystallogr. Sect. C*, **63**, 358 (2007).
- [45] N.F. Chilton, R.P. Anderson, L.D. Turner, A. Soncini, K.S. Murray. *J. Comput. Chem.*, **34**, 1164 (2013).